JCTC Journal of Chemical Theory and Computation

Article

pubs.acs.org/JCTC

Photostability Mechanisms in Human γB-Crystallin: Role of the Tyrosine Corner Unveiled by Quantum Mechanics and Hybrid Quantum Mechanics/Molecular Mechanics Methodologies

Marco Marazzi,*[,†] Isabelle Navizet,[‡] Roland Lindh,[§] and Luis Manuel Frutos*[,†]

[†]Departamento de Química Física, Universidad de Alcalá, E-28871 Alcalá de Henares (Madrid), Spain

[‡]School of Chemistry, University of the Witwatersrand, ZA-2050 Johannesburg, South Africa

[§]Department of Chemistry, Ångström, The Theoretical Chemistry Programme, Uppsala University, SE-75120 Uppsala, Sweden

Supporting Information

ABSTRACT: The tyrosine corner is proposed as a featured element to enhance photostability in human γB-crystallin when exposed to UV irradiation. Different ultrafast processes were studied by multiconfigurational quantum chemistry coupled to molecular mechanics: photoinduced singlet−singlet energy, electron and proton transfer, as well as population and evolution of triplet states. The minimum energy paths indicate two possible UV photoinduced events: forward−backward proton-coupled electron transfer providing to the system a mechanism for ultrafast internal conversion, and energy transfer, leading to fluorescence or phosphorescence. The obtained results are in agreement with the available experimental data, being in line with the proposed photoinduced processes for the different tyrosine environments within γB-crystallin.

INTRODUCTION

Crystallins are the main proteins forming the vertebrate eye lens, reaching 90% of the total protein content in the human eye lens.[1] Light passes through the cornea, the barrier between the external environment and the inside of the eye, and is focused by the lens on the retina, which contains the necessary photoreceptors to initiate the transmission of the optic information to the brain via nerve cells.[2,3]

α-, β-, and γ-crystallins (the three main types of crystallin) are not subject to protein turnover during a whole lifetime. Thereby the high stability showed against UV/vis irradiation is responsible for the long-term transparency of the eye lens. Changes in the crystallin structure can cause precipitation of protein aggregates in the lens cells.[4] As a result, light is largely blocked by the lens and the optical information does not reach the retina anymore. This phenomenon is known as a cataract, the major cause of blindness worldwide.[5]

Therefore a major challenge is to understand which chemical mechanisms can be considered responsible for a stable transparency of the crystallin. In other words, what kind of molecular or atomistic processes can prevent the eye lens from being damaged from the UV irradiation present in sunlight? In order to attempt possible answers to this question, all UV photostability mechanisms should be taken into account, since they could play a prominent role. Here we focus attention on the structural proteins of the eye lens, i.e., β- and γ-crystallins, characterized by high similarity: they are both formed by domains consisting of two Greek-key motifs (Figure 2). Different photostability mechanisms were already proposed: as a biological mechanism, α-crystallin was shown to bind in vitro partially unfolded proteins preventing aggregation,[6−8] therefore suggesting that α-crystallin can prevent aggregation of partially damaged or unfolded β- and γ-crystallins (i.e., prevent cataract formation).[9]

Evidently, other photostability mechanisms would be more efficient if β- and γ-crystallins could maintain their structures without undergoing partial unfolding. Especially, ultrafast internal conversion could allow conversion of the excitation energy into vibrational energy. The dissipation of the extra energy by the environment could permit the system to finally reach the ground state (GS), restoring the initial electronic structure of the system. β- and γ-crystallins contain tryptophan (Trp) and tyrosine (Tyr) residues that can act as UV filters, protecting the retina by absorbing at wavelengths $\lambda < 315$ nm (energy > 3.94 eV) in the case of Trp, and $\lambda < 300$ nm (energy > 4.13 eV) in the case of Tyr (Figure 1). Trp has shown intrinsic fluorescence in different proteins.[10,11] In human γD- and γS-crystallins, Trp fluorescence is quenched in the native state, but small changes in the protein conformation around Trp could result in a loss of efficiency of the fluorescence quenching mechanism.[12−15] The fluorescence quenching results from ultrafast mechanisms acting on Trp and its environment, such as fast electron transfer mechanisms, as has been shown by experiments and computations,[14−16] and it may protect the lens proteins from ultraviolet photodamage. The much wider match between γB-crystallin[17] and Tyr fluorescence emission spectra, instead of γB-crystallin and Trp fluorescence emission spectra,[18] is an indication that Trp fluorescence quenching is a relevant process. Moreover, Tyr residues can cause phosphorescence of γ-crystallins, although the presence of specific quenchers can decrease it.[19]

Nevertheless, additional mechanisms for ultrafast internal conversion could act on Tyr residues, furnishing additional pathways to enhance photostability. Especially the Tyr corner is a highly conserved conformational element in all β- and γ-crystallin domains,[21,22] where a Tyr side chain is hydrogen bonded to the

Received: February 8, 2012
Published: February 28, 2012

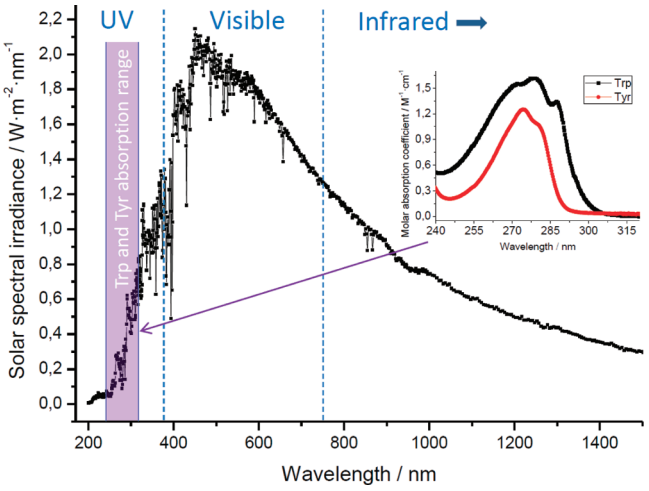

Figure 1. Solar spectrum subdivided into UV, visible, and infrared regions.[20] Tryptophan and tyrosine UV absorption spectra are shown as an inset.[18]

protein backbone (see Figures 2 and 3). Hydrogen bonds between amino acids were proposed as featuring elements to

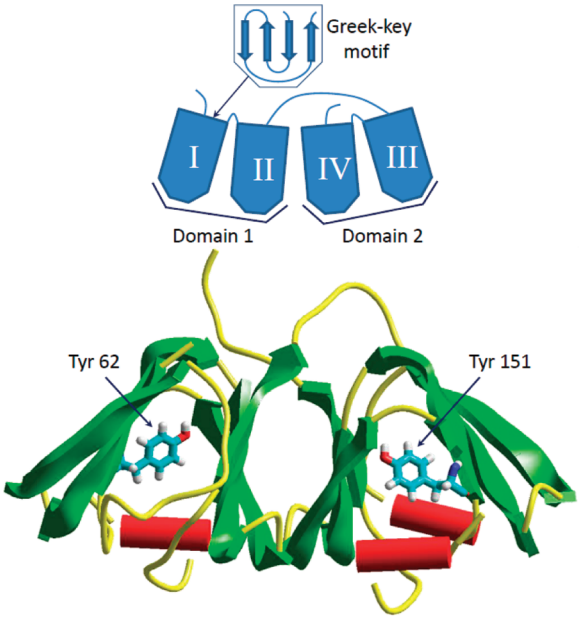

Figure 2. Schematic view of the γ-crystallin tertiary structure, with Greek-key motif I depicted (top). Human γB-crystallin structure and its Tyr corners (bottom). PDB code: 2JDF.

confer photostability to proteins via a photoinduced proton transfer (PPT) mechanism:[23−26] in a first (forward) step photoinduced electron transfer promotes the proton transfer along the hydrogen bond coordinate, resulting in a net transfer of a hydrogen atom. A second (backward) step permits reforming the initial hydrogen bond pattern in picoseconds, via a back electron transfer which promotes a back proton transfer.[27,28]

Especially proton-coupled electron transfer from Tyr and phenol (the Tyr chromophore) systems was proposed by theoretical studies[29] and observed experimentally,[30−33] including different possible mechanisms: stepwise electron transfer followed by proton transfer (PPT), stepwise proton transfer

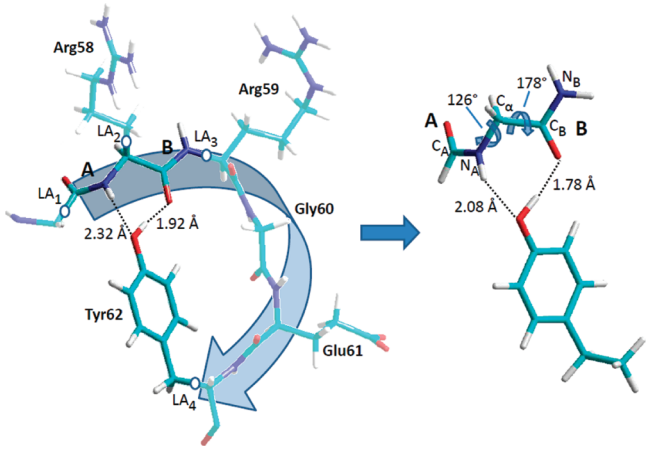

Figure 3. GS optimized structures at the CASSCF level (12 electrons in 10 orbitals). In both QM/MM (left) and QM (right) models the $C_A-N_A-C_\alpha-C_B$ and $N_A-C_\alpha-C_B-N_B$ dihedrals were kept constant at 126 and 178°, respectively (crystallographic structure).

followed by electron transfer, and a concerted mechanism where the hydrogen atom is transferred in a single step.

The aim of this study is to evaluate the role of the Tyr corner as a conformational element enhancing photostability. In order to understand how (and to what extent) the protein environment affects each photoinduced mechanism, we performed quantum mechanics (QM) and quantum mechanics/molecular mechanics (QM/MM) calculations on a Tyr-corner model as a self-assembling unit and as a model taking into account the surrounding human γB-crystallin (see Figure 3). The possible photoinduced pathways in the Tyr corner indicate PPT and energy transfer as possible competitive mechanisms conferring photostability to the eye lens.

METHODS

The study is focused on the calculation of the excited states of the Tyr-corner structure, a conformational element present in all structural crystallins, characterized by stable hydrogen bonds which could give rise to ultrafast internal conversion as a possible deactivation process of the incoming UV irradiation on earth (see Figure 1). In order to obtain a mechanistic description of the relevant photophysical processes, ab initio multiconfigurational methods were applied to a QM model of the hydrogen-bonded moiety within the Tyr corner as a standalone system and as a QM region of a QM/MM model including the whole human γB-crystallin (Figure 3). More in detail, considering its successful results in describing quantitatively the energies and electronic structure of several molecular systems, the MS-CASPT2//SA-CASSCF[34] methodology was applied to the system studied in this work.[35,36] (see Supporting Information for computational details).

Minimum energy paths (MEPs) were calculated at the SA-CASSCF level, permitting location of the energy minima on the potential energy surfaces (PESs) under study.

When two different singlet states were found to be degenerate in energy, the resulting crossing was characterized by calculating the nonadiabatic coupling vectors (i.e., derivative coupling (DC) and gradient difference (GD) vectors), in order to determine the crossing topology: for avoided crossings (ACs), GD and DC vectors are parallel, thus providing the initial direction of the reaction coordinate of the process, while for conical intersections (CIs), GD and DC vectors generate a

two-dimensional branching space where the energy degeneracy is left.

An active space of 12 electrons in 10 orbitals was selected, including four orbitals on the Tyr side chain (two π and two π^* on the aromatic ring) and three orbitals on each of the two peptide bonds of the backbone (one π, one π^*, and one n orbital on the C═O). In order to validate the employed active space, a more extended study was performed to determine the absorption spectrum, by considering additionally two larger active spaces: 14 electrons in 12 orbitals, adding one π and one π^* orbital on the aromatic ring of the Tyr side chain, and 16 electrons in 13 orbitals, adding also one n orbital on the oxygen atom of the Tyr side chain (see Supporting Information for parameter details and main orbitals involved). For all atoms a 6-31G(d) basis set was adopted.

After the study of the QM model was performed by CASPT2//CASSCF methodology, the role of the protein environment and surrounding water molecules was considered by setting up a QM/MM model at the CASPT2//CASSCF/AMBER level, applying the AMBER99SB force field (see Supporting Information for a description of the methodology and model details).[37,38]

More in detail, the backbone strand selected for a quantum chemical treatment in the QM/MM model includes the two peptide bonds, A and B, directly involved (by the hydrogen bonds with the Tyr side chain) in a description of the possible photoinduced mechanisms. Three hydrogen link atoms (LA_1 to LA_3) were needed to define the QM/MM frontier for the selected backbone, while LA_4 permits including the Tyr62 side chain in the QM region. This results in a QM region of the size appropriate for a CASPT2//CASSCF treatment.

The QM model, properly constrained to mimic the Tyr-corner conformation (see Supporting Information), includes all the features described for the QM region of the QM/MM model, allowing for a comparison of the photoinduced processes feasibility in vacuo and within the native protein environment (see Figure 3).

All calculations for the QM model were performed with Molcas 7[39] and Gaussian 03[40] packages. The setup of the MM model was carried out with the Tinker 4.2 software.[41] The QM/MM calculations were performed with the Molcas 7.6/Tinker 4.2 interface.

RESULTS AND DISCUSSION

Ground-State Structure. The Tyr corner is a conformational element which usually acts as a β-arch connecting two consecutive β-strands: in β- and γ-crystallins the Tyr corner connects two Greek-key motifs (see Figure 2). The Tyr corner is commonly formed by a short sequence of four, five, or six residues having always Tyr as the C-terminal amino acid. The Tyr-corner element is usually stabilized by a hydrogen bond placed between the OH group of the Tyr side chain and the backbone CO group of the first residue of the corner sequence (i.e., a Tyr—OH···O═C pattern). Additionally, a second hydrogen bond can be formed between the oxygen of the Tyr side chain and the backbone NH group of the first residue of the corner structure (i.e., a Tyr—O···H—N pattern).

All β- and γ-crystallins contain two almost identical Tyr-corner elements. Especially in human γB-crystallin the two Tyr-corner sequences (Arg58-Arg59-Gly60-Glu61-Tyr62 and Arg147-Pro148-Gly149-Glu150-Tyr151) differ only in the second residue of the sequence, favoring in both cases the formation of two hydrogen bonds between Tyr and the first residue of the corner (Tyr62···Arg58 and Tyr151···Arg147, respectively).

In this study attention is focused on the description of the interaction between the Tyr62 side chain and the backbone, via a QM minimal model of the Tyr corner and a hybrid QM/MM model where the Tyr62 corner is the QM center surrounded by the rest of human γB-crystallin, treated at the MM level (see Figure 3).

Absorption Spectra. The Franck—Condon (FC) main electronic transitions, CASPT2 vertical excitation energies (ΔE), and oscillator strengths (f) of the singlet excited states up to 8 eV are shown in Table 1. As expected, UV absorption by the phenol group (Ph) of the Tyr side chain ($S_0 \rightarrow S_1$) is the highest probability transition, within the biologically relevant middle-UV region (from ca. 4.1 to 6.2 eV), which could initiate any photophysical process: the f value of the $^1(\pi,\pi^*)_{Ph}$ transition corresponding to a single excitation to the lowest locally excited state (LE_1) is from 1 to 2 orders of magnitude larger than the f values of the $^1(n,\pi^*)_A$ and $^1(n,\pi^*)_B$ dark states.

Table 1. CASPT2 (16 Electrons in 13 Orbitals) Absorption Spectra of the QM and QM/MM Models[a]

state	transition	ΔE_{QM}/eV	$\Delta E_{QM/MM}$/eV	$f_{QM} \times 10$	$f_{QM/MM} \times 10$
S_6 (CT)	$^1(\pi_{Ph} \rightarrow \pi^*_B)$	7.11	7.21	12.834	16.038
S_5 (LE_5)	$^1(\pi,\pi^*)_{Ph}$	7.06	7.08	0.218	0.766
S_4 (LE_4)	$^1(\pi,\pi^*)_{Ph}$	6.04	6.54	0.141	0.177
S_3 (LE_3)	$^1(n,\pi^*)_B$	6.03	6.49	0.007	0.010
S_2 (LE_2)	$^1(n,\pi^*)_A$	5.89	6.17	0.006	0.010
S_1 (LE_1)	$^1(\pi,\pi^*)_{Ph}$	4.84	4.81	0.357	0.245

[a] S_0, corresponding to the GS at the Franck—Condon point, is the energy reference: $\Delta E = E(S_n) - E(S_0)$.

Higher in energy, both QM and QM/MM absorption spectra show LE states associated with the $^1(\pi,\pi^*)_{Ph}$ transition (LE_4 and LE_5), and a charge transfer (CT) state corresponding to a $^1(\pi_{Ph} \rightarrow \pi^*_B)$ transition. Direct population of the CT state is favored by a high f value and would lead to electron transfer from the Tyr side chain to the backbone, but the high energy required for the transition (ΔE_{QM} = 7.11 eV, $\Delta E_{QM/MM}$ = 7.21 eV) makes the event not likely to happen in the FC region.

In the following sections, the possible excited-state relaxation pathways are investigated and the resulting processes are organized as follows: first all singlet—singlet energy, electron, and proton transfer processes are detailed for the QM model, followed by a section dedicated to the role of triplet states. Once all possible mechanisms are shown in vacuo, a comparison with the photoinduced processes in the QM/MM model is made, in order to elucidate the effect of the protein environment on the Tyr-corner element.

Energy Transfer Processes. After vertical transition to the first excited state corresponding to the Tyr side chain (LE_1, $^1(\pi,\pi^*)_{Ph}$), the first photophysical process which could take place is energy transfer to the crystallin backbone: an LE_2/LE_1 singlet—singlet state crossing is found between the lowest bright $^1(\pi,\pi^*)_{Ph}$ state and the dark $^1(n,\pi^*)_A$ state, corresponding to a conical intersection (CI). Two different pathways are possible after the crossing: on one side, the eventual population of the LE_2 state could allow ultrafast energy transfer from Tyr to peptide bond A, finally reaching a minimum where the O_{Tyr}···HN_A hydrogen bond is increased from 2.08 to 2.28 Å (see Figure 4). The DC vector at

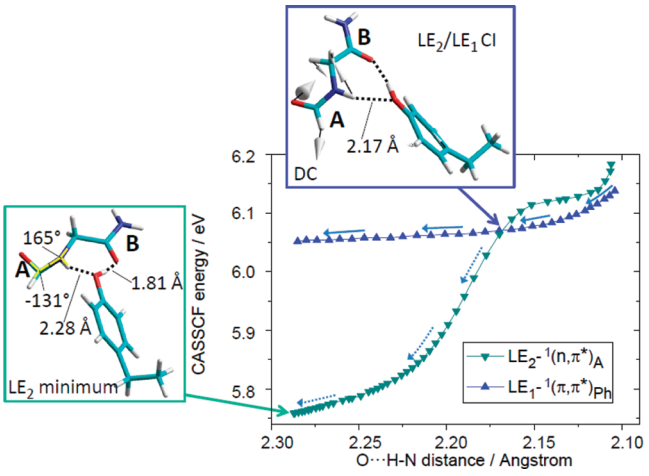

Figure 4. CASSCF MEPs of LE_1 and LE_2 states in the QM model after FC-vertical excitation, corresponding to LE_1 energy stabilization (solid arrows) or ultrafast energy transfer at LE_2/LE_1 CI ($O_{Tyr}\cdots HN_A$ distance = 2.17 Å), followed by LE_2 minimization (dashed arrows). The corresponding DC vector is shown.

the LE_2/LE_1 CI and the LE_2 minimum structure show clearly the driving force in the relaxation process: while the B moiety keeps the H−N−C−O planarity, the A moiety undergoes pyramidalization over the carbon and nitrogen atoms of the peptide bond.

The topology of the PESs near the CI suggests that the coupling between LE_1 and LE_2 states should be not strong enough to make efficient the population of LE_2, thus favoring LE_1 energy stabilization instead of LE_2 population. Both electronic states energies are in fact slightly avoided in the branching space close to the CI, indicating the low efficiency of the crossing.

On the other hand, if the system is further stabilized in the LE_1 state, an excited-state intermediate is reached which evolves giving rise to a second process where the O_{Tyr}—H···O=C_B hydrogen bond is the main reaction coordinate: after the LE_2/LE_1 CI, LE_1 decreases in energy reaching a minimum at an O_{Tyr}—H···O=C_B distance around 1.55 Å. From this minimum, a transition state is found at 5.49 kcal·mol^{-1}, at the CASPT2 level (see Figure 5). The vibrational excess on LE_1 (more than 37 kcal·mol^{-1})[42] can be considered reasonably large to overcome this excited-state energy barrier, thereby leading to a second crossing between LE_1 and LE_2 (O_{Tyr}—H···O=C_B distance = 1.16 Å), corresponding to an AC in which the proton is almost transferred. Again both events (i.e., LE_1 further stabilization and energy transfer from Tyr to A, through LE_2 population) are possible competitive processes, in this case implying coupling of the C_A=O and in-plane aromatic ring stretching modes, as indicated by the parallel nonadiabatic coupling vectors (Figure 5, LE_1/LE_2 AC). If the dark $^1(n,\pi^*)_A$ state is populated, a minimum is then found on LE_2, corresponding to the same geometry found by the first described energy transfer process. A similar geometric change of the peptide bond was already found by the authors in a hydrogen-bonded two-glycine model, where the same mechanism proposed here (an AC between a $^1(\pi,\pi^*)$ and a $^1(n,\pi^*)$ state) could permit ultrafast energy transfer.[35]

Further evolution of the $^1(n,\pi^*)_A$ state could involve radiative decay to S_0, or a transition to the first triplet state (T_1, see Role of Triplet States).

Energy transfer processes from the Tyr side chain to B or between A and B were not found. The only possibility of populating the dark $^1(n,\pi^*)_B$ state (LE_3) is directly by absorption in the FC region, an unlikely event considering the low f value and the high energy required (see Table 1 and Supporting Information for details of the LE_3 evolution).

Electron and Proton Transfer Processes. Electron transfer processes are possible if the CT state can be populated, leading to transfer of negative charge from the aromatic ring to the B moiety. Especially the CT state is stabilized in energy along the O_{Tyr}—H···O=C_B proton transfer coordinate, crossing in turn with LE_2 and LE_1 states (Figure 5).

Therefore, electron transfer enhances the proton transfer already initiated in the LE_1 state, permitting ultimately the complete transfer in the CT state: once the CT state is populated, further stabilization in energy along the proton transfer coordinate allows an ultimate crossing with GS, where a backward electron transfer is followed by a backward proton transfer, reestablishing the initial electronic configuration (see Scheme 1).

Since the CT state cannot be populated by absorption in the FC region, efficient crossing with LE states constitute the bottleneck of any electron transfer process in the Tyr corner. A second requirement which should be fulfilled is a low energy barrier on the LE states, in order to increase the feasibility of the process.

An analysis of the nonadiabatic coupling vectors of the CT/LE_1 CI (Figure 5) clarifies that the proton on the Tyr side chain tends to detach from the phenol moiety and attach to the

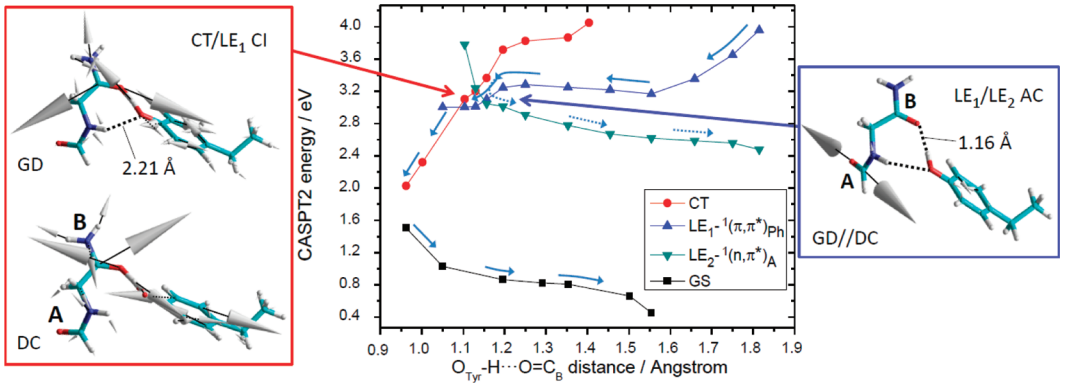

Figure 5. CASPT2 energy profile as a function of the O_{Tyr}—H···O=C_B hydrogen bond distance (QM model), starting from the LE_2 minimum (O_{Tyr}—H···O=C_B distance = 1.81 Å). Two UV-induced ultrafast processes are proposed: proton transfer (solid arrows) and energy transfer (dashed arrows). The nonadiabatic coupling vectors of CT/LE_1 CI (|GD| ≈ 18 |DC|) and LE_1/LE_2 AC (parallel vectors) are shown.

Scheme 1. Photoinduced Forward−Backward (f−b) Electron Transfer (ET) and Proton Transfer (PT) Mechanism, Suggested To Provide Photostability to the Tyr Corner of Human γB-Crystallin

$$\begin{array}{ccc} [\,TyrOH\cdots O{=}CR] & \xrightarrow[\text{f-ET}]{h\nu} & [\,TyrOH^{+}\cdots O^{-}{=}CR] \\ \text{b-PT}\uparrow & & \downarrow\text{f-PT} \\ [\,TyrO^{-}\cdots H^{+}O{-}CR] & \xleftarrow[\text{b-ET}]{} & [\,TyrO\cdots HO{-}CR] \end{array}$$

oxygen of the negatively charged B moiety, minimizing the charge separation. This causes rearrangements on the aromatic ring (which tends to adopt the configuration of a semiquinone) and on the B peptide bond (where CO and CN bonds tend to become single bonds).

An alternative pathway for electron and proton transfer implies population of the LE_2 state, which in turn could cross the CT state (CT/LE_2 AC, Figure 6). Even though the non-

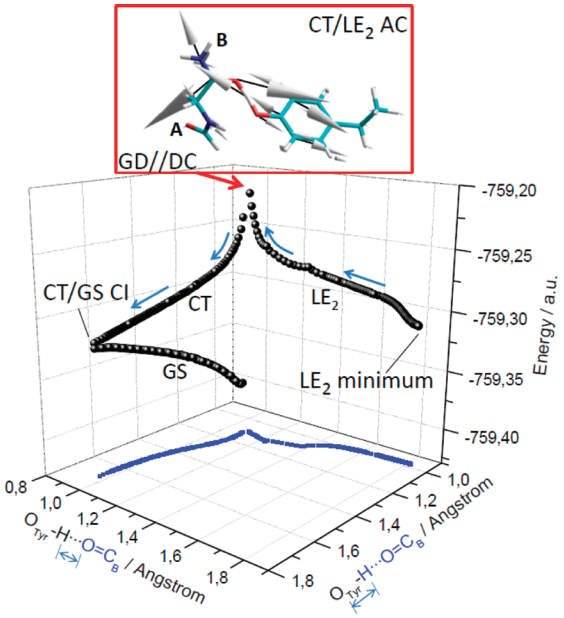

Figure 6. CASSCF MEPs calculated for CT and LE_2 states indicating electron and proton transfer (solid arrows) through a CT/LE_2 AC (GD parallel to DC). The potential energy is plotted as a function of O_{Tyr}—H···O=C_B hydrogen bond and O_{Tyr}–H bond distances.

adiabatic coupling vectors are similar to those found at the CT/LE_1 CI, the high energy barrier on the LE_2 state (ca. 36 kcal·mol^{-1}) makes the process not likely to happen.

Once the CT state is populated, the system undergoes vibrational relaxation, minimizing its energy and completing the proton transfer to the B moiety, ultimately reaching a CI with the GS state, corresponding to an S_1/S_0 CI (Figure 7). As indicated by the energy profile of CT and GS states around the CI, on the branching plane where energy degeneracy is left, two possibilities are given to the system when decaying to the GS state, corresponding to the energy minima along the loop (at ca. 70° for GS and 235° for CT): on one side, the GS state can be populated, transferring one electron from the B moiety to the Tyr side chain (as indicated by the Mulliken charges calculated around the CI). On the other side, the CT state can further decrease in energy, stabilizing the hydrogen-transferred electronic configuration. The nonadiabatic coupling vectors confirm this description and give the initial relaxation directions

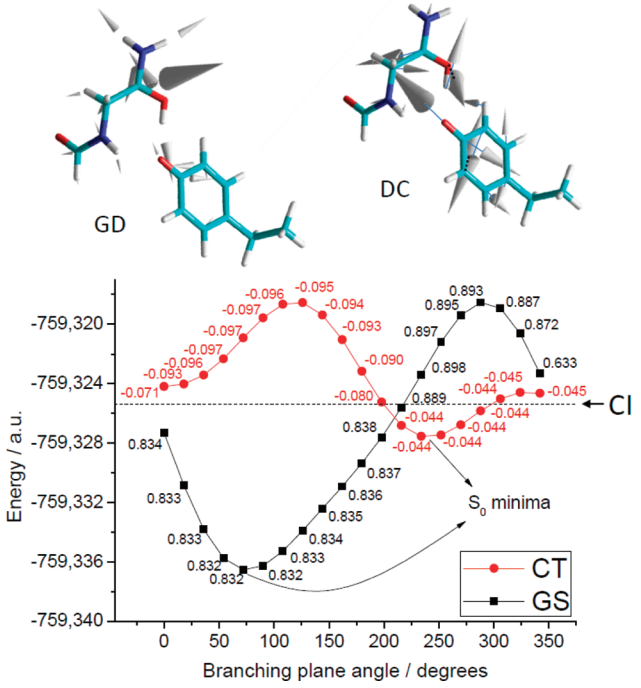

Figure 7. Energy of CT and GS states along a loop generated around the CT/GS CI (radius 0.05 Å) on the branching plane defined by the nonadiabatic coupling vectors (|GD| ≈ 53 |DC|). Mulliken charges, determined for the B moiety with contribution of the transferred hydrogen atom, are shown for both states at each point of the loop.

on S_0, with the transferred hydrogen on B pointing back to the Tyr side chain (GD vector) or being stabilized on the B moiety (DC vector).

The MEPs calculated from the CT/GS CI are shown in Figure 8: if the GS state is directly populated, the proton just

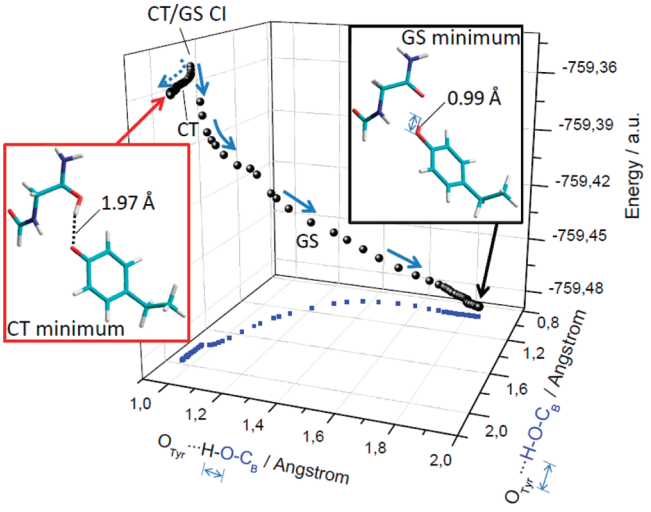

Figure 8. MEPs on S_0 after CT/GS CI, indicating back proton transfer from B to the Tyr side chain, reforming the initial FC structure (solid arrows), or formation of a metastable hydrogen-transferred photoproduct (dashed arrows).

formed on B migrates back to the Tyr side chain, reestablishing the initial Tyr-corner structure, therefore providing photostability. As an additional pathway, a minimum on the CT state is found ca. 6 kcal·mol^{-1} lower than the CT/GS CI, where the

dx.doi.org/10.1021/ct300114w | J. Chem. Theory Comput. 2012, 8, 1351−1359

OH hydrogen bond between semiquinone and B moieties enlarges to 1.97 Å. This hydrogen-transferred species should correspond to a metastable photoproduct, since the high vibrational excess on the CT state (see at Figure 5 the steepness of the CT energy profile) can be sufficient to overcome the low energy barrier between the CT minimum and the CT/GS CI, allowing for population of the GS state which promotes back electron and proton transfer.

Role of Triplet States. Triplet states also play a role for the photostability of the Tyr-corner structure: when irradiating the system (FC region), the low spin−orbit coupling between GS and triplet states excludes direct excitation to a triplet state and suggests that an excited singlet state will be populated, most probably corresponding to LE_1 (see Table 1). Therefore, a triplet state can be formed only by a transition from an excited singlet state (i.e., by intersystem crossing). As previously discussed, the LE_1/LE_2 AC involves an energy transfer process, where the initially excited molecule (LE_1 state) has some probability of populating the $^1(n,\pi^*)_A$ state (LE_2), reaching a minimum at an O_{Tyr}—H···O═C_B distance around 1.8 Å (Figure 5). From this stationary point an alternative pathway to radiative decay (i.e., fluorescence) is given by a possible transition to the $^3(n,\pi^*)_A$ state (T_1), where the minimum energy structure in this state is located as close as 5 kcal·mol^{-1} below the LE_2 state. The structural and energy proximity of LE_2 and T_1 minima as well as the nonvanishing spin−orbit coupling (0.15 cm^{-1})[43] ensures that the $^3(n,\pi^*)_A$ state can be populated. Once the $^3(n,\pi^*)_A$ state is populated, two different mechanisms can be proposed: phosphorescence from the T_1 minimum and evolution along the triplet states.

The energy profile shown in Figure 9 suggests that, in principle, the triplet states can undergo the same forward−backward

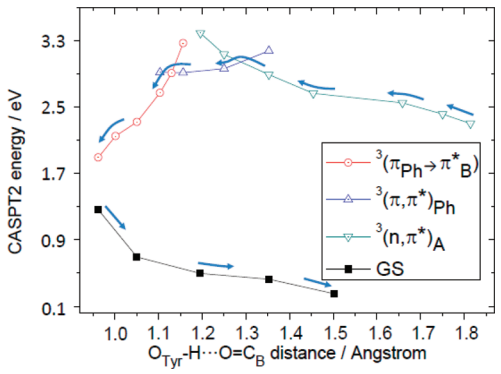

Figure 9. QM model CASPT2 energy profile of the triplet states possibly involved in PPT (mechanism showed by arrows). The proposed pathway implies population of the $^3(n,\pi^*)_A$ state at O_{Tyr}—H···O═C_B distance around 1.8 Å, a $^3(n,\pi^*)_A/^3(\pi,\pi^*)_{Ph}$ crossing, population of a triplet CT state through a $^3(\pi,\pi^*)_{Ph}/^3(\pi_{Ph} \rightarrow \pi^*_B)$ crossing, and finally decay to the GS state.

proton-coupled electron transfer process: a $^3(n,\pi^*)_A/^3(\pi,\pi^*)_{Ph}$ crossing between triplet LE states permits reaching a second $^3(\pi,\pi^*)_{Ph}/^3(\pi_{Ph} \rightarrow \pi^*_B)$ crossing, where a triplet CT state can be populated, corresponding to electron transfer from the Tyr side chain to B (as for the singlet CT). The charge separation is stabilized by proton transfer to B, by which an ultimate $^3(\pi_{Ph} \rightarrow \pi^*_B)$/GS crossing is reached, allowing for ultrafast internal conversion.

The factor limiting the feasibility of PPT by triplet states is the energy barrier on the $^3(n,\pi^*)_A$ state (from the $^3(n,\pi^*)_A$ minimum to the $^3(n,\pi^*)_A/^3(\pi,\pi^*)_{Ph}$ crossing), which was estimated to be 29 kcal·mol^{-1}.

Effect of the Protein Environment. Excited-state deactivation pathways were calculated for a QM/MM model, where the active center, which corresponds to the QM model studied in vacuo, is now surrounded by the protein and water molecules (Figure 10).

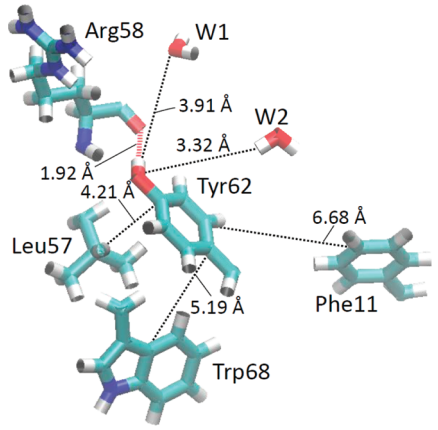

Figure 10. Side chains (Phe11, Leu57, Arg58, and Trp68) and the water molecules (W1 and W2) surrounding Tyr62, as defined by the ground-state optimized QM/MM geometry.

The photoinduced energy, electron, and proton transfer processes depicted for the QM model were found also in the QM/MM model, with differences in energy and structure which affect the efficiency of the mechanism of photostability (the most relevant structures are given in the Supporting Information).

Both possibilities described in the QM model to populate the dark $^1(n,\pi^*)_A$ state after irradiation to the bright $^1(\pi,\pi^*)_{Ph}$ state (through crossings between LE_1 and LE_2) were found also in the QM/MM model. Especially two LE_1/LE_2 crossings could imply migration of energy from the initially excited Tyr side chain to peptide bond A (see Figure 11). Just after vertical excitation from GS to LE_1, a first LE_1/LE_2 crossing is found,

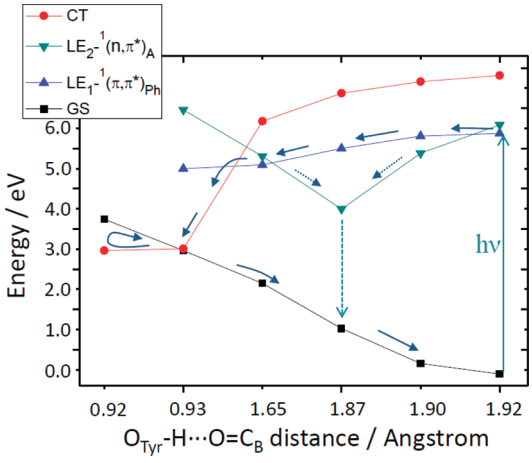

Figure 11. Energy profile of the possible UV photoinduced mechanisms in a human γB-crystallin QM/MM model, as a nonlinear function of the O_{Tyr}—H···O═C_B distance: forward−backward proton-coupled electron transfer (solid arrows) and energy transfer followed by fluorescence (dashed arrows).

dx.doi.org/10.1021/ct300114w | J. Chem. Theory Comput. 2012, 8, 1351−1359

while a second possibility to populate LE_2 is located at an O_{Tyr}—H···O═C_B distance around 1.65 Å. For the first crossing (lower vibrational excess), the probability of nonadiabatic transition was estimated to be 0.12, while for the second crossing (higher vibrational excess), the probability decreases to 3.60×10^{-5}, as indicated by Landau−Zener theory (see Supporting Information).

This means that the originally populated $^1(\pi,\pi^*)_{Ph}$ state (LE_1) first crosses with the $^1(n,\pi^*)_A$ state (LE_2) with a minor but still relevant probability of transferring energy to LE_2, and preferentially continuing to descend in energy up to the second cross with LE_2, where the population of the $^1(n,\pi^*)_A$ state is a much less likely event, leading to electron transfer via a CT state population.

Comparing QM and QM/MM models, two main differences were found:

1. No intermediate was found in the QM/MM model for the LE_1 state after vertical excitation. Therefore, no energy barrier is present in this state, making more efficient the subsequent photophysical processes predicted for this state. On the contrary, an energy barrier of 5.49 kcal·mol^{-1} was found for the QM model (see Figures 5 and 11).
2. The crossing between LE_1 and LE_2 states corresponds to different structures for QM and QM/MM models: in the QM model, considering the O_{Tyr}—H···O═C_B hydrogen bond coordinate, the hydrogen atom is almost transferred to peptide bond B (Figure 5, at 1.16 Å), while in the QM/MM model the same hydrogen atom is still distant from peptide bond B: 1.92 and 1.65 Å for the first and second crossings, respectively (see Figure 11). This suggests that Dexter-type singlet−singlet energy transfer is a competitive process when the protein environment is included, while proton-coupled electron transfer is highly preferred in the Tyr corner as a standalone moiety.

In the QM/MM model, the population of the CT state through a CT/LE_1 crossing corresponds to migration of one electron from the Tyr side chain to peptide bond B, followed by transfer of a proton to minimize the charge separation. This corresponds to stabilization of the CT state up to crossing with the GS. At the CT/GS crossing two processes can occur: a back proton-coupled electron transfer from peptide bond B to the Tyr side chain, restoring the initial GS geometry (FC region), or further stabilization of the CT state, where a metastable photoproduct, corresponding to net transfer of a hydrogen atom from the Tyr side chain to peptide bond B (CT minimum), was found ca. 4.5 kcal·mol^{-1} lower in energy than the CT/GS crossing. Since the same kind of hydrogen-transferred photoproduct was found in the QM model ca. 6 kcal·mol^{-1} lower in energy than the CT/GS crossing (see Figure 8), it can be concluded that a lower vibrational excess on the CT state is required for the QM/MM model to overcome the energy barrier between the CT minimum and the CT/GS crossing, therefore populating the GS and enhancing ultrafast internal conversion.

Singlet−singlet energy transfer leads to a $^1(n,\pi^*)_A$ minimum, characterized by pyramidalization over the carbon and nitrogen atoms of peptide bond A (−149 and 171°, respectively), as in the QM model (−131 and 165° respectively; see Figure 4, LE_2 minimum), but indicating lower deviation from the peptide bond planarity. Also in the QM/MM model, the eventual population of a triplet state from the $^1(n,\pi^*)_A$ minimum was considered as a possible alternative to fluorescence: a $^3(n,\pi^*)_A$ state is located ca. 9 kcal·mol^{-1} higher in energy, suggesting a possible but not prominent role of the triplet states eventually leading to phosphorescence (as indicated by experimental studies)[19] and therefore indicating fluorescence as the most important photophysical process after energy transfer. Especially fluorescence is calculated to take place at 4 eV (310 nm), mostly corresponding to the expected value for Tyr fluorescence in water (303 nm).[18] Considering the protein environment around the Tyr corner (see Figure 10), the proximity of Trp68 to Tyr62 suggests a possible fluorescence quenching mechanism through Förster resonance energy transfer between the two chromophores, a common event in proteins. Once the energy is transferred to Trp68, fluorescence quenching can follow, as suggested by theoretical and experimental studies showing the efficiency of Trp fluorescence quenching within γ-crystallin.[14−17]

Nevertheless, singlet−singlet energy transfer was estimated to be not prominent, as the highest probability for the process to happen was calculated to be 0.12 (LE_2/LE_1 crossing associated with low vibrational excess). Therefore, proton-coupled electron transfer is the most probable process within the Tyr-corner element of γB-crystallin (Figure 11 and Scheme 2, left), a process

Scheme 2. Energy Profiles of the UV Photoinduced Processes within the Tyr Residues of γB-Crystallin, Indicating by Arrows the Most Probable Mechanism: Ultrafast Radiationless Deactivation for Hydrogen-Bonded Tyr-Corner Elements (Left) and Fluorescence Radiative Decay for Tyr Residues Not Involved in Hydrogen Bonds (Right)

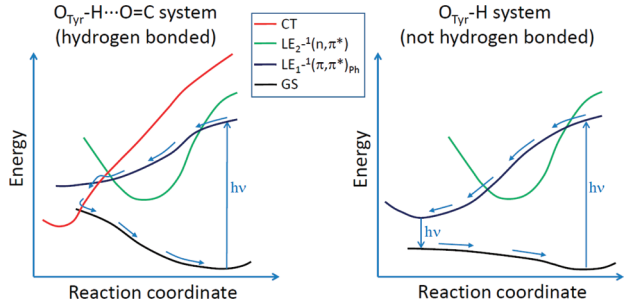

which can be proposed on the basis of theoretical and experimental findings.[29−33] This ultimately suggests that both Tyr-corner elements present in γB-crystallin can enhance the photostability of the human eye lens. Anyway, other Tyr residues are present in γB-crystallin not arranged as Tyr corners, therefore are not involved in hydrogen bonds with the protein backbone, and finally leading to photochemical pathways not including CT states (Scheme 2, right): proton-coupled electron transfer is not possible, while the most probable UV photoinduced event is fluorescence from the LE_1 minimum. This can explain fluorescence spectra recorded in γB-crystallin, where Tyr fluorescence quenching does not have a prominent role:[17] non-hydrogen-bonded Tyr residues produce fluorescence, while Tyr-corner elements provide the necessary conformation to release the UV irradiation energy by ultrafast radiationless deactivation.

CONCLUSIONS

The absorption spectrum and excited-state deactivation pathways of a Tyr-corner model in vacuo and as part of human γB-crystallin were studied by means of quantum mechanics (CASPT2//CASSCF level) and hybrid quantum mechanics/

dx.doi.org/10.1021/ct300114w | J. Chem. Theory Comput. 2012, 8, 1351−1359

molecular mechanics (CASPT2//CASSCF/AMBER level) methodologies, respectively. Different photoinduced processes were described, including energy, electron, and proton transfer for both models. Among them, energy transfer and especially forward−backward photoinduced proton transfer were found to play relevant roles in enhancing UV photostability. More in detail, Dexter-type singlet−singlet energy transfer was shown to possibly play a significant role when considering the Tyr corner within the protein environment, finally leading to fluorescence from an originally dark $^1(n,\pi^*)$ state, or Förster resonance energy transfer to a Trp residue, followed by Trp fluorescence quenching. Energy transfer processes compete with radiationless forward−backward proton-coupled electron transfer, which was shown to be the prominent UV photoinduced process within the human γB-crystallin environment of the Tyr corner. When looking at the Tyr corner as a standalone system, energy transfer mechanisms are even less significant, although fluorescence from a $^1(n,\pi^*)$ state or phosphorescence from a $^3(n,\pi^*)$ state is still possible, and therefore favoring the competing mechanism: radiationless forward−backward proton-coupled electron transfer. Ultimately, both energy transfer and forward−backward proton-coupled electron transfer mechanisms could provide (at least partially) an explanation for the characteristic photostability of the eye lens when exposed to UV irradiation. A transition state on the locally excited $^1(\pi,\pi^*)$ state, initially activated by irradiation, defines a ca. 5.5 kcal·mol^{-1} barrier as the only limiting factor for photostability when in vacuo. Including the protein environment, no energy barriers were found on the potential energy surfaces involved in proton transfer (LE_1, CT, GS), thereby allowing ultrafast internal conversion. Apart from direct recovery of the initial structure (through a conical intersection with the ground state, CT/GS CI), a hydrogen-transferred species was found in both models as a metastable photoproduct of charge transfer character. A small vibrational excess (ca. 4.5 kcal·mol^{-1} in the case of the biologically relevant model) permits reaching again the CT/GS CI where back electron transfer is followed by back proton transfer, restoring the Franck−Condon geometry.

From the biological point of view, the description of the above-mentioned photoinduced processes suggests, when compared to available experimental studies, that the Tyr corner is a conformational element which can induce or enhance photostability against UV irradiation, therefore indicating the possibility of modifying an existing protein by including one or more Tyr-corner elements, in order to avoid UV photodamage. The residues surrounding the Tyr corner will be critical in enhancing energy transfer mechanisms toward proton-coupled electron transfer mechanisms, or vice versa.

In the eye lens, the presence of two mostly identical Tyr-corner elements in all γ-crystallins and the similarity of all β- and γ-crystallins (grouped together as βγ-crystallins superfamily) raises the probability that this structural moiety can play an effective role. Semiclassical trajectories of the studied QM/MM system could be proposed in order to provide additional information, especially related to the time scale and quantum yield of the different possible mechanisms.

■ ASSOCIATED CONTENT

Supporting Information

CASPT2//CASSCF methodology and computational details. QM/MM methodology and model details. Absorption spectra additional parameters. Description of the $^1(n,\pi^*)_B$ state evolution. Description of the energy transfer probability calculation. Cartesian coordinates of the most relevant structures. This material is available free of charge via the Internet at http://pubs.acs.org.

■ AUTHOR INFORMATION

Corresponding Author

*E-mail: marco.marazzi@uah.es (M.M.); luisma.frutos@uah.es (L.M.F.). Tel.: +34 91 885 2512. Fax: +34 918854763.

Notes

The authors declare no competing financial interest.

■ ACKNOWLEDGMENTS

This research was supported by the Spanish MICINN Grant CTQ2009-07120. M.M. is grateful to the UAH for a doctoral fellowship and a short-term scholarship spent in the Uppsala University. I.N. thanks Prof H. M. Marques for funding through the DST/NRF SARChI initiative. L.M.F. acknowledges receipt of a "Ramon y Cajal" contract from MEC. We thank Alexandra Ryazanova from Lomonosov Moscow State University for helpful discussions on biological aspects of the system studied.

■ REFERENCES

(1) Oyster, C. W. *The Human Eye: Structure and Function*; Sinauer Associates: Sunderland, MA, 1999; pp 595−647.
(2) Davson, H. *Physiology of the Eye*, 5th ed.; The Macmillan Press Ltd.: London, U.K., 1990; pp 105−138.
(3) Bermann, E. R. *Biochemistry of the Eye*, 1st ed.; Plenum Press: New York, 1991; pp 201−290.
(4) Benedek, G. *Invest. Ophthalmol. Vis. Sci.* **1997**, *38*, 1911−1921.
(5) Clark, J. I. *Principle and Practice of Ophthalmology*; Saunders College Publishing: Philadelphia, PA, 1994; pp 114−123.
(6) Horwitz, J. *Proc. Natl. Acad. Sci. U.S.A.* **1992**, *89*, 10449−10453.
(7) Merck, K. B.; Groenen, P. J.; Voorter, C. F.; de Haard-Hoekman, W. A.; Horwitz, J.; Bloemendal, H.; de Jong, W. W. *J. Biol. Chem.* **1993**, *268*, 1046−1052.
(8) van Boekel, M. A.; Hoogakker, S. E.; Harding, J. J.; de Jong, W. W. *Ophthalmic Res.* **1996**, *28S*, 32−38.
(9) Bloemendal, H.; de Jong, W.; Jaenicke, R.; Lubsen, N. H.; Slingsby, C.; Tardieu, A. *Prog. Biophys. Mol. Biol.* **2004**, *86*, 407−485.
(10) Eftink, M. R. *Methods Biochem. Anal.* **1991**, *35*, 127−205.
(11) Callis, P. R.; Liu, T. *J. Phys. Chem. B* **2004**, *108*, 4248−4259.
(12) Phillips, S. R.; Borkman, R. F. *Curr. Eye Res.* **1988**, *7*, 55−59.
(13) Kosinski-Collins, M. S.; Flaugh, S. L.; King, J. *Protein Sci.* **2004**, *13*, 2223−2235.
(14) Chen, J.; Flaugh, S. L.; Callis, P. R.; King, J. *Biochemistry* **2006**, *45*, 11552−11563.
(15) Chen, J.; Callis, P. R.; King, J. *Biochemistry* **2009**, *48*, 3708−3716.
(16) Chen, J.; Toptygin, D.; Brand, L.; King, J. *Biochemistry* **2008**, *47*, 10705−10721.
(17) Mayr, E.-M.; Jaenicke, R.; Glockshuber, R. *J. Mol. Biol.* **1997**, *269*, 260−269.
(18) Du, H.; Fuh, R. A.; Li, J.; Corkan, A.; Lindsey, J. S. *Photochem. Photobiol.* **1998**, *68*, 141−142.
(19) Mandal, K.; Chakrabarti, B. *Biochemistry* **1988**, *27*, 4564−4571.
(20) ASTM G173-03(2008). *Standard Tables for Reference Solar Spectral Irradiances: Direct Normal and Hemispherical on 37° Tilted Surface*; ASTM International: West Conshohocken, PA, 2008.
(21) Hemmingsen, J. M.; Gernert, K. M.; Richardson, J. S.; Richardson, D. C. *Protein Sci.* **1994**, *3*, 1927−1937.
(22) Hamill, S. J.; Cota, E.; Chothia, C.; Clarke, J. *J. Mol. Biol.* **2000**, *295*, 641−649.
(23) Frutos, L. M.; Markmann, A.; Sobolewski, A. L.; Domcke, W. *J. Phys. Chem. B* **2007**, *111*, 6110−6112.
(24) Sobolewski, A. L.; Domcke, W. *J. Phys. Chem. A* **2007**, *111*, 11725−11735.

(25) Shemesh, D.; Sobolewski, A. L.; Domcke, W. *J. Am. Chem. Soc.* **2009**, *131*, 1374−1375.
(26) Marazzi, M.; Sancho, U.; Castaño, O.; Domcke, W.; Frutos, L. M. *J. Phys. Chem. Lett.* **2010**, *1*, 425−428.
(27) Schultz, T.; Samoylova, E.; Radloff, W.; Hertel, I. V.; Sobolewski, A. L.; Domcke, W. *Science* **2004**, *306*, 1765−1768.
(28) Lan, Z.; Frutos, L. M.; Sobolewski, A. L.; Domcke, W. *Proc. Natl. Acad. Sci. U.S.A.* **2008**, *105*, 12707−12712.
(29) Sobolewski, A. L.; Domcke, W. *J. Phys. Chem. A* **2001**, *105*, 9275−9283.
(30) Sjödin, M.; Styring, S.; Wolpher, H.; Xu, Y.; Sun, L.; Hammarström, L. *J. Am. Chem. Soc.* **2005**, *127*, 3855−3863.
(31) Görner, H.; Khanra, S.; Weyhermüller, T.; Chaudhuri, P. *J. Phys. Chem. A* **2006**, *110*, 2587−2594.
(32) Malval, J.-P.; Diemer, V.; Morlet-Savary, F.; Jacques, P.; Chaumeil, H.; Defoin, A.; Carré, C.; Poizat, O. *J. Phys. Chem. A* **2010**, *114*, 2401−2411.
(33) Swarnalatha, K.; Rajkumar, E.; Rajagopal, S.; Ramaraj, R.; Banu, I. S.; Ramamurthy, P. *J. Phys. Org. Chem.* **2011**, *24*, 14−21.
(34) Finley, J.; Malmqvist, P.-Å; Roos, B. O.; Serrano-Andres, L. *Chem. Phys. Lett.* **1998**, *288*, 299−306.
(35) Marazzi, M.; Sancho, U.; Castaño, O.; Frutos, L. M. *Phys. Chem. Chem. Phys.* **2011**, *13*, 7805−7811.
(36) Merchán, M.; Serrano-Andrés, L.; Fülscher, M. P.; Roos, B. O. *Recent Advances in Multireference Methods*; Hirao, K., Ed.; Recent Advances in Computational Chemistry 4; World Scientific Publishing Co.: Singapore, 1999; pp 161−195.
(37) Dapprich, S.; Komárino, I.; Byun, K. S.; Morokuma, K.; Frich, M. J. *J. Mol. Struct. (THEOCHEM)* **1999**, *461*, 1−21.
(38) Humbel, S.; Sieber, S.; Morokuma, K. *J. Chem. Phys.* **1996**, *105*, 1959−1967.
(39) Aquilante, F.; De Vico, L.; Ferré, N.; Ghigo, G.; Malmqvist, P.-Å.; Neogrády, P.; Pedersen, T. B.; Pitoňák, M.; Reiher, M.; Roos, B. O.; Serrano-Andrés, L.; Urban, M.; Veryazov, V.; Lindh, R. *J. Comput. Chem.* **2010**, *31*, 224−247.
(40) Frisch, M. J.; Trucks, G. W.; Schlegel, H. B.; Scuseria, G. E.; Robb, M. A.; Cheeseman, J. R.; Montgomery, J. A., Jr.; Vreven, T.; Kudin, K. N.; Burant, J. C.; Millam, J. M.; Iyengar, S. S.; Tomasi, J.; Barone, V.; Mennucci, B.; Cossi, M.; Scalmani, G.; Rega, N.; Petersson, G. A.; Nakatsuji, H.; Hada, M.; Ehara, M.; Toyota, K.; Fukuda, R.; Hasegawa, J.; Ishida, M.; Nakajima, T.; Honda, Y.; Kitao, O.; Nakai, H.; Klene, M.; Li, X.; Knox, J. E.; Hratchian, H. P.; Cross, J. B.; Adamo, C.; Jaramillo, J.; Gomperts, R.; Stratmann, R. E.; Yazyev, O.; Austin, A. J.; Cammi, R.; Pomelli, C.; Ochterski, J. W.; Ayala, P. Y.; Morokuma, K.; Voth, G. A.; Salvador, P.; Dannenberg, J. J.; Zakrzewski, V. G.; Dapprich, S.; Daniels, A. D.; Strain, M. C.; Farkas, O.; Malick, D. K.; Rabuck, A. D.; Raghavachari, K.; Foresman, J. B.; Ortiz, J. V.; Cui, Q.; Baboul, A. G.; Clifford, S.; Cioslowski, J.; Stefanov, B. B.; Liu, G.; Liashenko, A.; Piskorz, P.; Komaromi, I.; Martin, R. L.; Fox, D. J.; Keith, T.; Al-Laham, M. A.; Peng, C. Y.; Nanayakkara, A.; Challacombe, M.; Gill, P. M. W.; Johnson, B.; Chen, W.; Wong, M. W.; Gonzalez, C.; Pople, J. A. *Gaussian 03*, revision C.02; Gaussian, Inc.: Wallingford, CT, 2004.
(41) Tinker Molecular Modeling, version 4.2; http://dasher.wustl.edu/tinker/ (accessed Feb 27, 2012).
(42) The vibrational excess is calculated as the energy difference from the LE_1 $^1(\pi,\pi^*)_{Ph}$ vertical absorption (FC region) to the LE_1 minimum (O_{Tyr}—H···O═C_B hydrogen bond distance around 1.55 Å).
(43) The spin−orbit coupling (i.e., $\langle T_1|H|S_1\rangle$) was calculated considering the CASPT2 energy difference between T_1 and S_1 states at the LE_2 minimum and applying atomic mean-field integrals.